

J. Environ. Treat. Tech. ISSN: 2309-1185

Journal web link: http://www.jett.dormaj.com https://doi.org/10.47277/JETT/9(3)697



Removal of Phenol from Aqueous Solution by Adsorption onto Baobab Fruit Shell Activated Carbon: Equilibrium and Kinetics Studies

Radhia Nedjai, Nassereldeen Ahmed Kabbashi*, Ma'an Fahmi Rashid Alkhatib, Md Zahangir Alam

Department of Biotechnology Engineering, Faculty of Engineering, International Islamic University Malaysia, P.O Box 10, 50728 Kuala Lumpur, Malaysia

Abstract

Phenol compounds are considered one of the major problems faced by many countries owing to their release in wastewaters from various industries. These pollutant compounds are harmful to marine life and human beings. Therefore, in the present study, Baobab Fruit Shells (BFS) were used as a precursor for the production of activated carbons for the removal of phenol. The chemical activation of BFS using ZnCl₂, H₃PO₄, and KOH with an impregnation ratio of 1:1 at 500 °C for 1 h in Nitrogen (N₂) atmosphere was investigated. The effects of these chemicals on the performances of the prepared activated carbons (yield, surface area, adsorption properties) were studied. Fourier transform infrared (FT-IR), scanning electron microscope (SEM), X-ray diffraction (XRD), and N₂ adsorption analyses were performed for the characterization of BFS-ACs. SEM results showed that porous structures were formed on the surface of different sizes. FTIR analyses show the presence of different surface groups on the activated carbons. The highest BET surface area and micropore volume were obtained by KOH with 1029.435 m²/g and 0.369 cm³/g, respectively. The developed BFS-ACs were used for the removal of phenol from the aqueous solution. The results indicated KOH in terms of adsorption and efficiency showed better results with a maximum adsorption capacity of 36.90 mg/g at a higher initial concentration (600 mg/L). The adsorption rate of phenol by BFS-ACs was rapid and more than 95.02 % phenol could be absorbed by KOH-AC within the initial 15 min. Phenol adsorption behavior can be described by the Langmuir isotherm model and the pseudo-second-order kinetics. This study provided an effective source that could be used in the production of activated carbon for the treatment of wastewaters as it could be attained at a low cost.

Keywords: Activated Carbon, Baobab Fruit shell, Chemical Activation, Phenol Adsorption, Kinetics & isotherms adsorption

1 Introduction

Phenol compounds are considered a major problem faced by many countries due to their release in wastewaters by various industries such as petroleum refineries, petrochemical, pharmaceuticals, pesticide manufacturing, synthetic resins, steel mills, coke manufacturing, coal gas, paints, wood pulp production, dyes production and mine discharge [1-3]. Besides, they are also present in the wastewater of agro-industrial processes such as the palm oil mill effluent, olive oil mills, wine distilleries, and tomato processing [4]. Phenols were commonly used industrially because they may be used as intermediate chemicals in a large variety of applications [3, 5]. Phenol is currently produced worldwide at a rate of approximately 7.8 million tons per year, with a considerably growing trend [6]. The presence of these pollutants in waterways may negatively influence the environment as well as human health, food chain, and marine life owing to their high bio-accumulation rate and their toxic effects [7]. Therefore, before releasing the phenol to receiving waters, it should be treated.

Various conventional and advanced techniques have been applied to eliminate phenolic compounds from aqueous solutions. Conventional techniques include ion-exchange [8–10], absorption, distillation [11], chemical oxidation [12, 13], coagulation [14, 15], extraction [16], biodegradation [17] and electrochemical oxidation [18], adsorption technique utilizing natural and synthetic zeolites [19], fly ash [20], activated clay [21], and activated carbon [22]. While advanced techniques include Fenton processes, ozonation, catalytic wet oxidation [23], and photochemical treatment [24], which are based on the use of fewer chemicals than conventional methods. However, the use of high energy makes some of these methods very expensive [25]. Biological treatment such as anaerobic granular sludge [26] has the advantages of being energy-less and more environmentally friendly, but it cannot treat low concentration pollutions [25]. Studies on the treatment of effluent-bearing phenolic compounds and specifically phenol have revealed adsorption to be an extremely efficient technique for the removal of phenol from the pollutant water and activated carbons have been widely utilized

^{*}Corresponding author: Nassereldeen Ahmed Kabbashi, Department of Biotechnology Engineering, Faculty of Engineering, International Islamic University Malaysia, P.O Box 10, 50728 Kuala Lumpur, Malaysia; E-mail: nasreldin@iium.edu.my

as adsorbents. This absorbent received considerable attention owing to the benefits such as operational convenience and selectivity, high performance, superior design flexibility, and no generation of harmful by-products [27]. Despite its widespread use in water and wastewater treatment industries, activated carbon still an expensive substance [6]. Hence, there is needed to reduce the cost of production by using inexpensive and abundant raw materials which may be an efficient solution to the discarding of huge amounts of waste and minimize the production cost of activated carbon as well.

Lignocellulosic biomass has become one of the most important starting materials to produce activated carbon due to its benefits, especially for the environment [28]. Many studies have proposed the use of lignocellulosic wastes as suitable raw materials to prepare AC, such as coconut shells [29, 30], peanut shell [31, 32], sunflower seed [31], tobacco [33], olive stones [34], gelatin, starch [35], palm kernel shell [36], empty fruit bunch [37, 38], pistachio nut shells [39], neem husk [40], almond shell [39], jackfruit peel [41], fox nutshell [42], rice husk [43], Rubber seed shell [7], and baobab fruit shells [44–46]. These varieties of precursors are cheap, abundant, renewable, non-toxic, readily available, and environmentally friendly [28, 47, 48].

Baobab fruit shells contain 24.87% of cellulose and 54.08% of lignin, which contributed to high absorptivity characteristics in AC [46]. Baobab fruit shell (BFS) is one of the most abundant waste, with a share of 45% of the total weight of baobab fruit. Annually, averaging tree production amounted to 673,000 tonnes [46, 49], resulting in 30,285 tonnes of baobab fruit shell generated. During processing operations of baobab to pulp powder, seed oil, fruit juice, or other valuable products, significant amounts of baobab fruit shells are generated as waste without any economic benefit [50]. It is generally dumped nearby the harvesting and processing sites, therefore damaging the ecosystem. Hence, with baobab fruit shell waste is in abundance, an advanced process for converting BFS waste to a commodity with a more cost-effective benefit is required [50].

Recently, few studies have shown that activated carbon could be successfully synthesized from baobab fruit shells [45, 46]. It has been reported that activated carbon-based BFS has a high adsorption capacity for the removal of Cu(heavy metal)[44] and dye (MB)[45]. Therefore, the activated carbon produced from BFS could be applied as an adsorbent to remove the phenol.

The present work aims to illustrate the production of activated carbons derived from Baobab fruit shells, namely BFS, through the chemical activation using three different activating agents and to demonstrate their adsorptive capacities for phenol removal. Chemical activation has been selected since it presents several advantages over physical activation, such as a large surface area and great yield with low activation temperature and short activation time [51]. The chemical activation process has been carried out using an impregnation ratio of 1:1, activation temperature of 500 °C, and activation time of 1 hour, under a nitrogen (N₂) atmosphere. The lowest pyrolysis temperature (500°C) has been chosen to investigate the suitability of using a moderate value, which in conjunction with a suitable chemical treatment could result in a cost-effective preparation protocol. Moreover, it has been revealed that the optimum pyrolysis temperature for producing AC from lignocellulosic materials is 500 °C [52, 53]. Phenol adsorption was used to study the adsorption capacity of prepared activated carbons to remove organics from the wastewater. Fourier transforms infrared (FT-

IR), scanning electron microscope (SEM), and X-ray diffraction (XRD) techniques were used to characterize the produced activated carbon.

2 Material and Methods

2.1 Materials

The Baobab Fruit Shell (BFS), the precursor used in preparing activated carbons, was acquired from Kordofan State in North Sudan. Potassium hydroxide (KOH) and zinc chloride (ZnCl₂) were used as chemicals reagents for activation, which were purchased from Sigma-Aldrich and R&M Chemicals, Malaysia. phosphoric acid (H_3PO_4) was acquired from Macron Fine Chemicals, USA. High-purity (99.95%) nitrogen gas was obtained from Fuelink Marketing Sdn. Bhd., Selangor, Malaysia, which was used for the inert atmosphere during carbonization. All other chemicals of analytical grade were utilized during the experiments.

2.2 Adsorbate Preparation

Different concentrations of solutions were prepared using deionized water. 1000 mg/L of phenol solution was prepared by dissolving a suitable quantity of phenol (C_6H_5OH) with deionized water in the volumetric flask of 1 L. Then, the prepared solution was diluted with de-ionized water to get the needed concentrations, which are 50, 100, 200, 400, and 600 ppm.

2.3 Preparation of BFS-ACs

The BF shells were rinsed several times with tap water and lastly by distilled water to eliminate any impurities. The shells were dried at 105°C for 24 hours for dehydration until a constant mass was obtained. Then, samples were reduced by scissors in sizes less than 2 cm. Later, they were crushed using Mill MF 10 basic microfine grinder drive, IKA® WERKE, and sieved to a particle size of 1 mm using a sieve shaker AS 300 from Retsch. An amount of prepared raw baobab fruit shell was mixed with the chemical reagent (ZnCl2, H3PO4, or KOH) at an impregnation ratio of 1:1. An amount of distilled water was added which was equivalent to 4 times the total mass of the mixture. At 50 °C, the sample was agitated for 1 h utilizing Infors HT Ecotron shaking incubator, the sample was placed oven-dried overnight at 100 °C to get a thick paste. The mixture was placed in a reactor, which was continuously purged with high-purity N2 gas (99.95 %), and later was inserted into an electric horizontal tube furnace, where heated at 10 °C/min at 500 °C for 1 hour. The flow of the N2 gas continued to avoid carbon reacting with oxygen at high temperatures to produce CO₂ which could lead to a loss of carbon. The activated product was afterward moved from the furnace to the desiccator for cooling. The product mass was measured, and later was removed any ash in the sample and any residual of the dehydrating agents was dissolved through washing the activated carbon using 50 mL of 0.5M hydrochloric acid (HCl). A final product was frequently washed by warm distilled water until a constant pH was attained [54]. The activated carbon (AC) was inserted in an oven to dry for 48 hours at 110 °C. The AC sample was stored in a desiccator for further usage.

2.4 Physicochemical characterization of BFS-ACs 2.4.1 Proximate analysis

The moisture content of BFS-ACs was measured based on a procedure by ASTM D 2867-91 [55], and the ash content was

determined by ASTM D 2866-83 [56].

2.4.2 Yield

Activated carbons yields were calculated based on the next equation:

$$Yield(\%) = \frac{W_f}{W_i} \times 100 \tag{1}$$

where M_f is the dry mass of final activated carbon in grams, which is taken after the activated carbon is produced. While M_o is the dry mass of baobab fruit shells in grams, which is taken at the beginning of the experiment [41].

2.4.3 Characterization of BFS-AC

Physical adsorption of N_2 (at 77 k) was utilized to characterize the porosity of the BFS-ACs using Quantachrome, Autosorb-1C, and a surface area analyzer according to the Brunauer–Emmett–Teller (BET) model. Preceding the measurement, the samples utilized outgassed at 300°C for 4 hours under vacuum. The data have been subjected to certain mathematical analyses to obtain the surface area.

Fourier transform infrared (FT-IR) spectroscopic was applied to analyze the surface chemistry of the raw BFS and BFS-ACs prepared to utilize a Thermo Scientific NicoletTM model iS50 FT-IR Spectrometer. The morphological structure of the original raw material and the prepared activated carbon were observed using a JEOL-IT 100 SEM instrument. Before analyses, the samples were placed on double-sided carbon conductive tape. Pores size measurements have been determined using the measurement tool equipped with the JEOL IT100 SEM (InTouchScopeTM version 1.060).

X-ray diffraction patterns of the precursor and BFS-ACs were carried out using a Bruker D2 Phaser at 30kV and 10mA Cu K α radiation source (k=1.54184Å).

2.5 Batch Equilibrium Studies

Batch equilibrium adsorption experiments were achieved via different concentrations of phenol solution (50, 100, 200, 400, and 600 mg/L). Dry activated carbon (0.25g) was separately taken in several conical flasks and mixed with 25mL of phenol solution at different concentrations and agitated using a rotary shaker at a constant stirring speed of 200 rpm and room temperature (27±1°C) for various contact times (i.e. 5, 10, 15, 30, 60, 120, 180min). Then, the suspension was filtered, and the residual concentration of phenol was determined at 270 nm using a UV/vis spectrophotometer. All the experiments and analyses were conducted three times to minimize errors. At equilibrium time, the amount of phenol adsorbed by biosorbent was calculated using the following equation:

$$q_e = \frac{(c_i - c_f)v}{w} \tag{2}$$

where q_e : the amount of phenol adsorbed per gram of biosorbent at equilibrium (mg/g), C_i : the initial phenol concentration (mg/L), C_f : the equilibrium phenol concentration (mg/L), V: the volume

of phenol solution in the flasks (L), and W: the weight of biosorbent utilized (g) [57]. The difference between phenol concentration in the aqueous solution before and after adsorption (C_i-C_f) to the initial concentration of phenol (C_i) is known as the phenol removal percentage and can be measured utilizing equation 3.

Removal Percentage =
$$\frac{(C_i - C_f)}{C_i} \times 100$$
 (3)

3 Results and Discussion

3.1 Characterization of adsorbent (BFS-ACs)

Fourier transform infrared (FTIR), scanning electron microscopy (SEM), X-ray diffraction (XRD), and BET surface area analyses were carried out to characterize the BFS-ACs. Some physicochemical characterizations of BFS-ACs were done to comprehend the mechanism engaged in the procedure of adsorption such as the moisture content and ash content.

3.1.1 Ash & Moisture Content

Ash content and moisture content are important proprieties that affect the adsorption performance of the prepared activated carbon. Therefore, they were determined, and the results are illustrated in Table 1. Ash content consists of various useless mineral substances, which become more concentrated during the activation process. It primarily depends on the type of raw material and ranges from 1 to 20 %. High ash content is unsuitable for AC as it affects adsorptive capacity and decreases the mechanical strength of carbon [58]. The ash content values of the prepared activated carbons were almost similar, and it ranges from 14.3 to 17.7 %. Moisture content increases the weight and dilutes the carbon over the treatment process. Hence, the lower the moisture content, the preferable the activated carbon [30]. The moisture content for Zncl₂, and KOH activated carbons were as lower as 1.15 and 1.65 %, demonstrating good carbon.

3.1.2 Effects of Activating Agents on the Yield of FB-ACs

The production yields of activated carbons are also shown in Table 1. According to the results, the highest yield was obtained for 34.39% which was produced by phosphoric acid (H_3PO_4) , while the lowest yield for 30.37% was prepared by potassium hydroxide (KOH) under the same temperature $(500\ ^{\circ}C)$. This high temperature hurts the yields of BFS-ACs. It is expected because, baobab fruit shells are essentially formed of natural polymers like cellulose, lignin, and hemicellulose [46]. At higher temperatures, these polymeric structures decompose, and more volatiles are liberated causing a lower yield.

Table 1: Properties of BFS-ACs (prepared at carbonization temperature of 500 °C and impregnation ratio of 1:1 for 1 hour)

Adsorbent	Yield (%)	Moisture content (%)	Ash content (%)
$ZnCl_2$	33.66	1.15	17.3
H_3PO_4	34.39	5.17	17.7
KOH	30.37	1.63	14.3

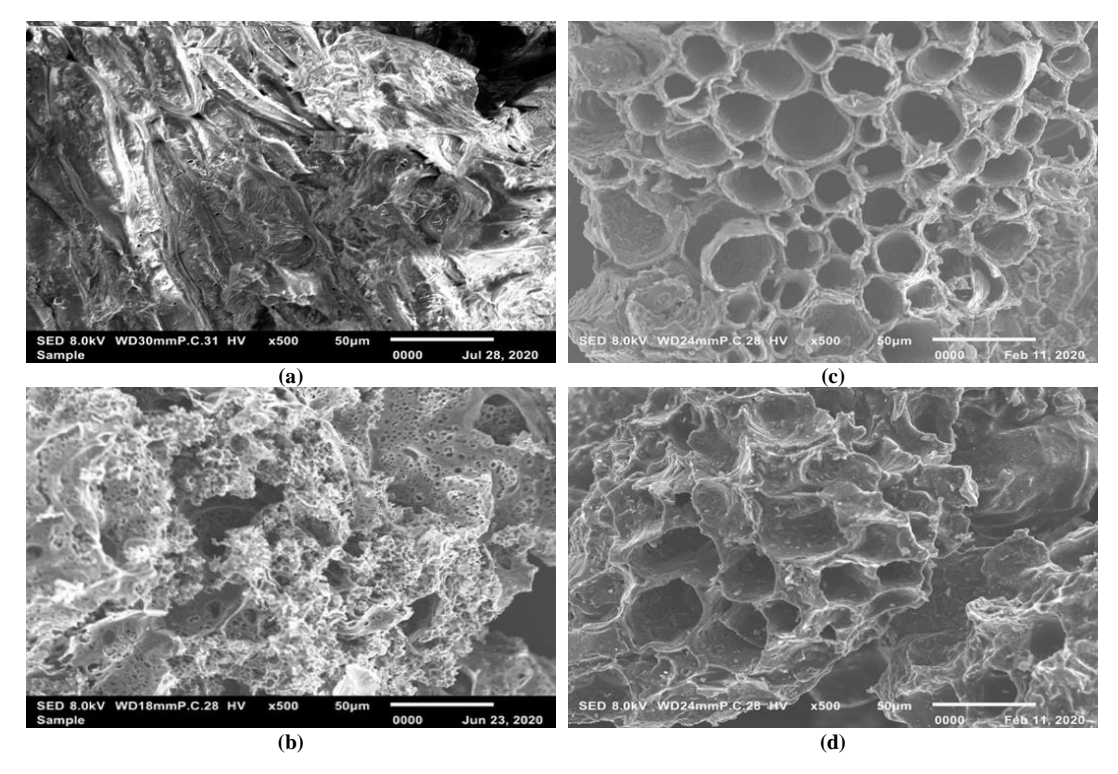


Figure 1: Morphological structure of BFS (a), and Activated Carbon impregnated with different activating agents (b) KOH, (c) H_3PO_4 , and (d) $ZnCl_2$ (magnification scale $\times 500$)

The yield obtained by H₃PO₄ is higher owing to the presence of H₃PO₄ during activation, which favors the transformation of aliphatic to aromatic compounds and promotes depolymerization, dehydration, and redistribution of constituent biopolymers, therefore, increasing the yield of activated carbon [41].

3.1.3 BET Surface Area

The surface area was calculated by the Brunauer, Emmett, and Teller (BET) equation [59] utilizing the N2 adsorption data. According to the results shown in Table 2, ZnCl₂-AC, H₃PO₄-AC, and KOH-AC presented high BET surface areas of 559.537 m²/g, 904.492 m²/g, and 1029.435 m²/g, respectively. The average size of the pores determines adsorbate molecules' ability to penetrate inside the AC, the adsorbed molecules penetrate the adsorbent only if pores have a diameter that is greater than the effective molecular diameter of the adsorbate [60]. The effective molecular diameter of phenol is 0.75 nm and the average pore sizes of ZnCl₂-AC, H₃PO₄-AC, and KOH-AC were 4.127, 3.061, and 1.676 nm, respectively, indicating that all BFS-ACs were suitable for the adsorption of phenol. From Table 2, it can be also seen that the KOH-AC is a highly developed micropore area of 940.878 m²/g, micropore volume of 0.369 cm³/g, a smaller external surface area of 88.556 m²/g, and a smaller pore diameter of 1.676 nm in comparison with ZnCl₂-AC and H₃PO₄-AC samples.

3.1.4 Scanning Electron Microscope (SEM)

The SEM technique was applied to observe the morphological surface of the un-activated BFS, and the resulting activated carbon was prepared with chemical activation methods using ZnCl₂, KOH, H₃PO₄. Figure 1 represents the results, which demonstrated a significant variance in the morphological surface

of the starting material and BFS-ACs. The surface morphology of the un-

Table 2: BET Surface Area of BFS-ACs

	Adsorbent	S_{BET}^{a} (m ² /g)	S_{Micro}^{b} (m ² /g)	S_{External}^{c} (m^{2}/g)	D_{pore}^{d} (nm)	V_t^e (cm ³ /g)	V_{Micro}^f (cm ³ /g)
_	ZnCl ₂	559.537	261.833	297.704		0.577	0.112
	H_3PO_4	904.492	413.320	491.172	3.061	0.692	0.182
	KOH	1029.435	940.878	88.556	1.676	0.431	0.369

^a BET specific surface area, ^b t-Plot Micropore Area, ^c t-Plot External Surface Area, ^d Adsorption average pore diameter, ^e Single point adsorption total pore volume of pores, ^f t-Plot micropore volume

activated material sample (Fig. 1 a) contains the lowest original pore structures. However, the micrographs (Fig 1 b, c, and d) show that when the BFS is treated with activating agents (ZnCl₂, KOH, H₃PO₄), more porous structures occur and constitute honeycomb with different pore structures. They have displayed those chemicals influenced the topographical characteristics of the surfaces of the carbon.

In general, it can be seen that there is a different texture of the morphological structure of prepared activated carbons with different pores sizes, which refer to the appearance of different reaction mechanisms. The mechanism of KOH is more complex and includes the disintegration (almost explosively) of the structure following intercalation and some gasification by oxygen molecules of hydroxide as well. Whereas, $ZnCl_2$ promoting the removal of H_2O molecules from the lignocellulosic structures of parent materials, and H_3PO_4 incorporating chemically inside the lignocellulosic structures. Therefore, there is no selective removal of carbon during activation which improves the yields [61].

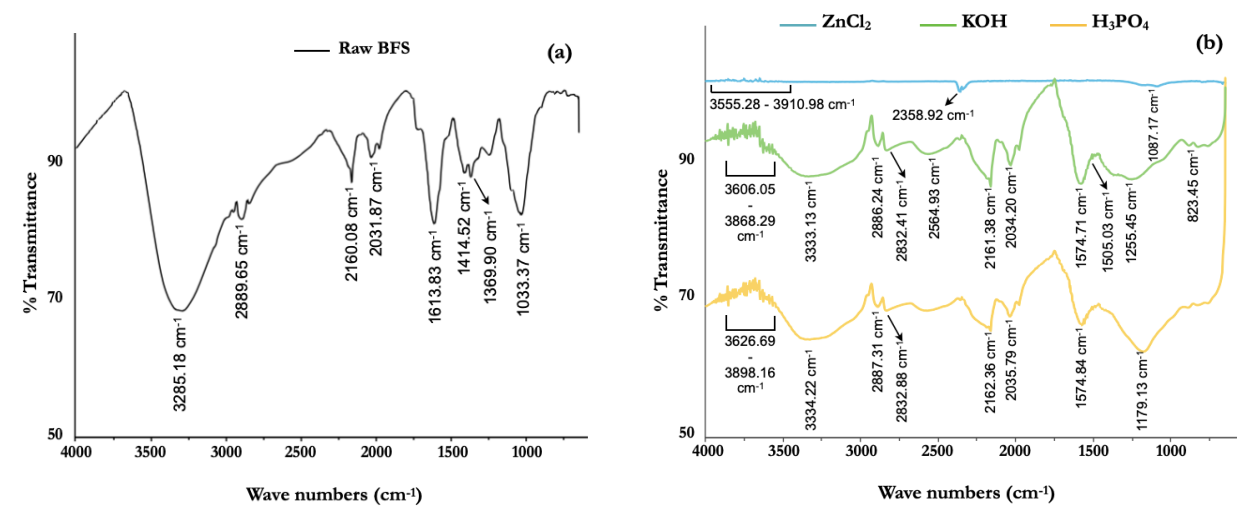


Figure 2. Fourier Transform Infra-Red Spectra for raw baobab fruit shells (a) and BFS-ACs (b)

H₃PO₄ and ZnCl₂ activated carbons (Fig. 1 c and d) obviously presented developed honeycomb as highly determined pores and cavities compared to raw BFS. But the pores are not uniform. On the other hand, the surface of KOH carbon (Fig. 1 b) is filled with many small pores. High macropore size is observed in ZnCl₂ activated carbons, followed by H₃PO₄ then KOH. Moreover, the number of pores present in the KOH micrograph is highest than those present in H₃PO₄ and ZnCl₂. Therefore, there is a high possibility of trapping and absorbing phenol in the presence of large pores.

3.1.5 Surface Chemistry

Fig. 2 shows the FT-IR spectra of un-activated baobab fruit shells (Fig. 2 a) and BFS derived activated carbons (Fig. 2 b). It can be seen that the raw material spectrum exhibited more bands than the AC spectrum, where several peaks existent in the baobab fruit shells disappeared after the activation step due to the elimination of volatiles and heat-sensitive functional groups at high temperature (500 °C). For the raw material (BFS), the broadband at 3285.18 cm⁻¹ was ascribed to the existence of hydrogen-bonded (O-H) groups of cellulose, pectin, and lignin [45]. The band appearing at around 2889.65 cm⁻¹ was attributed to (C-H) symmetric stretching and (-CH2) alkyl groups. The weak peaks observed at around 2160 cm⁻¹ and 2031 cm⁻¹ were due to the existence of $(C \equiv N)$ stretching. The peak at 1613.83 cm⁻¹ is the aromatic ring or the olefinic (C=C) stretching vibration due to carboxyl, lactone, ketones, and aldehyde [41, 44, 45], which is disappeared in activated carbons. A relatively low-intensity band at around 1367 cm⁻¹ was due to the presence of (C-O-C) stretching or C=C stretching that can be attributed to the existence of ester, ether, and phenol. The band situated at 1033.37 cm⁻¹ was the characteristics of anhydrides (C-O), which is observed in ZnCl₂ and disappeared completely in KOH and H₃PO₄. The major functional groups in BFS are hydroxyl groups, carbonyl groups, and carboxyl groups. All of activated carbons spectra display broad weak peaks around 3900–3600 cm⁻¹. For the zinc chloride activated carbon, very weak peaks around 2358 and 1087 cm⁻¹ ascribed to the presence of alkyls groups (C-H), and hydroxyls

(O–H). On the other hand, KOH and H₃PO₄ activated carbons present a similar FTIR spectrum, which indicates the identical type of surface functional groups. The bands at around 3333.13 cm⁻¹, 2886.24 cm⁻¹, 2161.38 cm⁻¹, 1574.71 cm⁻¹, 1255.45 cm⁻¹ were the characteristics of O–H (hydroxyls), C–H (alkyls), C≡C (alkyne), C–O–C (ester, ether and phenol) and C–O (anhydrides), respectively. However, H₃PO₄ presents bands with bigger intensity as contrasted to KOH, which also indicates a higher quantity of functional groups in H₃PO₄. According to Puziy et al., the brand obtained by H₃PO₄ at 1179.13 cm⁻¹ could be assigned to the phosphorous-containing group P–O, O–C stretching vibrations in P–O–C linkage, and P=OOH [62].

3.1.6 X-Ray Diffraction (XRD) Analysis

Activated carbons produced from BFS using different activating agents can be crystallographically characterized using XRD. The X-ray patterns of baobab fruit shell and BFS-ACs are shown in Figure 3.

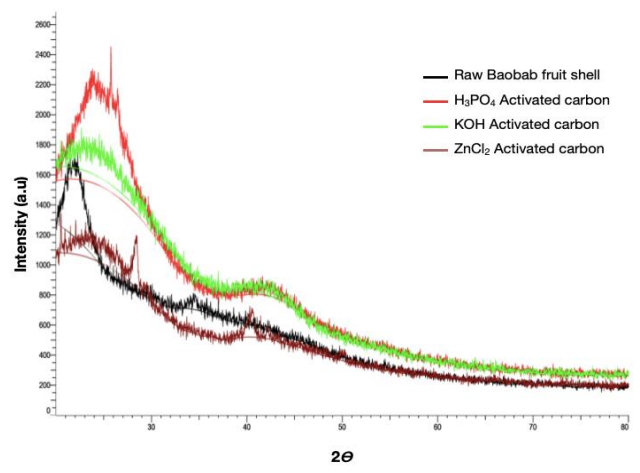


Figure 3: The XRD of raw BFS and prepared BFS-ACs

The diffraction profile displays a strong Bragg diffraction peak for raw material as well as activated carbons prepared in $2\theta = 20-30^{\circ}$ regions. The apparent extraordinary humps a high degree of disorder that are representative of carbonaceous materials. Moreover, there was no well-defined peak in any area of the diffraction profile, which indicates that the samples were not subject to any distinct mineral peaks. Similar findings and conclusions have been obtained from other studies [45, 63–65].

3.2 Adsorption Process

3.2.1 Effect of Initial Phenol Concentration

In this study, three different prepared activated carbons were employed as adsorbents to investigate the effect of chemical activating agents on phenol adsorption. Initial phenol concentration on the adsorption process is investigated by different initial phenol concentrations from 50 to 600 ppm and results are presented in Fig. 4. From the results, it can be seen that the actual amount of phenol adsorbed (mg/g) increased with an increase in the initial phenol concentration. When adding 10 g/L of activated carbon to phenol solution with a concentration of 600 mg/L, the amount of phenol adsorbed by KOH-AC, ZnCl₂-AC, and H₃PO₄-AC were 36.90, 14.27, and 9.75 mg/g, respectively. The results demonstrate that the phenol removal efficiencies of all three BFS-ACs have been different, especially at high concentrations. On the other hand, their efficiencies were almost similar at low concentrations.

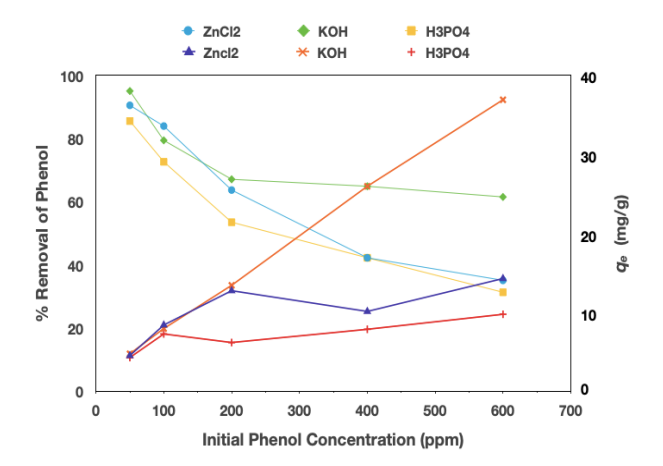


Figure 4: Effect of initial concentration on phenol adsorption (adsorbent dose = 10 g/L, agitation speed = 200 rpm, temperature = $27\pm1^{\circ}$ C)

Generally, the percentage of phenol removal decreased with the rise of the initial phenol concentration. The efficiency of the phenol removal by H₃PO₄-AC is mostly lower than that of ZnCl₂-AC as having been indicated by other researchers [43]. After 24 hours, the removal efficiency of up to 90 % could be attained at low concentration (50 mg/L) and up to 35 % at high concentration (600 mg/L) with 0.25 g ZnCl₂ activated carbon. Whereas the comparison between ZnCl₂-AC and KOH-AC displays that the efficiency of the uptake of phenol by KOH-AC is higher than that of ZnCl₂-AC. The efficiency of KOH-AC was reached 95.02 % at low concentration (50 mg/L) and 61.50 % at high concentration (600 mg/L). A considerable uptake of KOH compared to ZnCl₂-

AC and H₃PO₄-AC can be explained by differences in porosity and chemical surface, but many studies have attributed the main factor to this, is oxygen-containing functional groups that have a significant effect on phenol adsorption [43, 66, 67]. Where the decrease is primarily the cause of the increased phenol adsorption capacity in total functional groups which contain carb-oxygen. Usually, these functional groups typically appear as carboxylic, lactone base, and phenolic hydroxyl [67].

3.2.2 Effect of Contact Time

Fig. 5 (a-c) shows the effects of contact time on the adsorption of phenol onto BFS-ACs at different initial concentrations (50, 100, 200, 400, and 600 mg/L) at $27\pm1^{\circ}$ C. Adsorption studies were followed through for 3 hrs. In general, it can be seen that the adsorption capacity of phenol on BFS-ACs radically augmented during the initial period and then at a gradual speed. This due to the initial concentration, which provides a significant driving force that overcomes any mass transfer resistance [42]. The rising trend stopped once a state of equilibrium is attained. After the equilibrium stage, the quantity of phenol adsorbed is not changed considerably with time, which indicates that time is sufficient to achieve equilibrium for the maximum elimination of phenol from aqueous solutions by BFS-ACs.

Fig. 5 (a) shows that the time to attain equilibrium was observed to be 10 min for 50 and 100 mg/L, while this augmented to 30 min for a concentration of 400 and 600 mg/L. The adsorption equilibrium of phenol adsorption on ZnCl₂-AC augmented from 4.524 mg/g to 14.27 mg/g as the initial concentration of phenol augmented from 50 mg/L to 600 mg/L.

From Fig. 5 (b), a considerable amount of phenol was removed by KOH-AC in the first 15 min of contact time owing to the presence of a great number of empty sites on the surface of activated carbon. The adsorption capacity at equilibrium augmented from 4.751 to 36.90mg/g whereas the removal percentage was declined from 95.02 to 61.50 % with a rise in the initial phenol concentrations from 50 to 600 mg/L (see Fig. 4).

Phenol adsorption on the H₃PO₄-AC was a similar trend to that on the ZnCl₂-AC (Fig. 5 (c)). As observed, the adsorption equilibrium was reached in 30 min for all concentrations studied. After this time, there is no remarkable improvement was observed. The phenol adsorption capacity on BFS-ACs increases with increasing initial phenol concentration.

The sharp rises in the phenol absorption at initial stages could be explained in that BFS-ACs contain many accessible sites, whereas the decrease in the absorption of phenol once the equilibrium is reached indicates that BFS-ACs are become saturated at these levels. The results in Hameed et al. [68] study revealed that the equilibrium time needed for the phenol adsorption on rattan sawdust-based AC was almost 4 hrs.

However, the adsorption processes of this research were rapid and reached equilibrium in 30 min to 1hr based on the concentration of phenol. Similar results were also reported during the adsorption of phenol on activated carbon derived from palm oil empty fruit bunch and fox nutshell [37, 42]. This illustrates that BFS-ACs prepared have well-developed pores and highly active sites. Also, such observations have been reported by other investigators about the increase of the adsorbate concentration enhances the removal efficiency of phenol [2, 42, 68, 69].

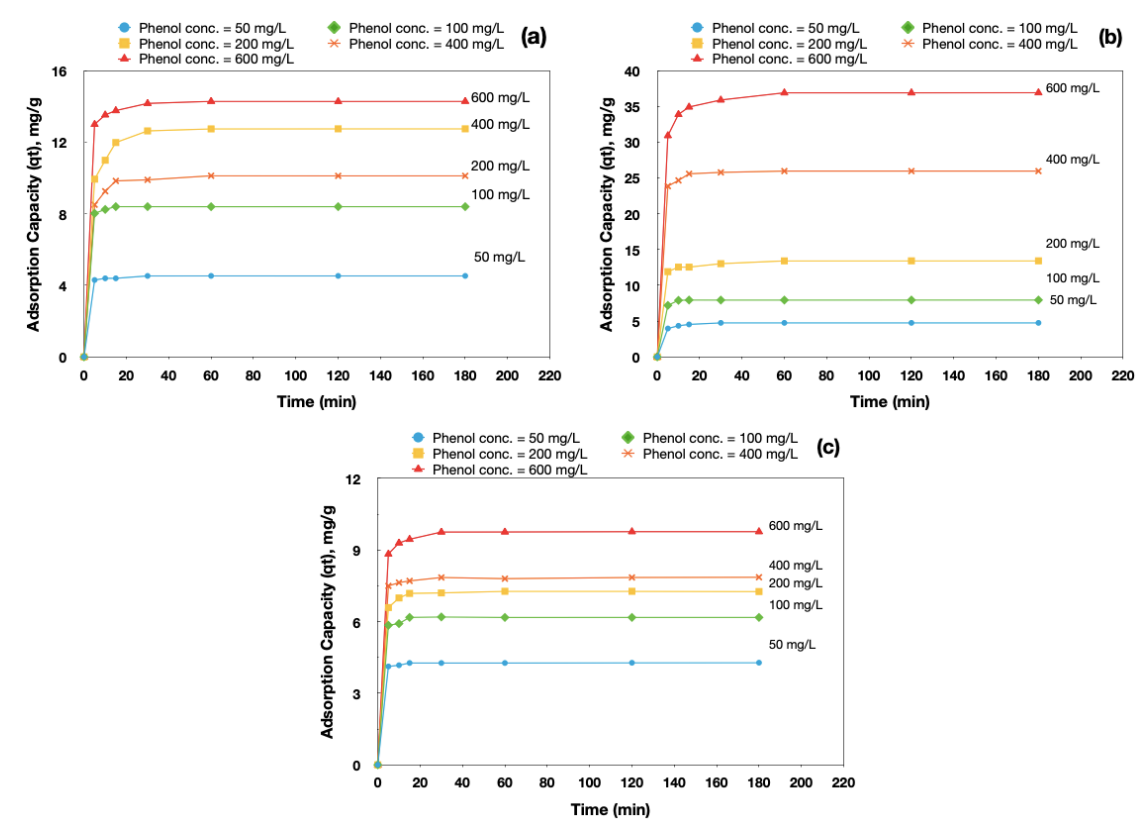


Figure 5: Effect of contact time on phenol adsorption (a) $ZnCl_2$ -AC, (b) KOH-AC, (c) H_3PO_4 -AC (adsorbent dose = 10 g/L, agitation speed = 200 rpm, temperature = 27 ± 1 °C)

3.3 Adsorption isotherms models

Isotherms of adsorption were used to demonstrate how the adsorbed molecules distribute between solid and liquid phases. For the adsorption system design, this is generally important [70]. Adsorption isotherm findings are usually displayed as a plot of the adsorbed concentration of the chemical (mg/g) relative to the rest of the solution (mg/L). The adsorption equilibrium data were modeled on the isotherms of Langmuir and Freundlich in this analysis.

3.3.1 Langmuir isotherm

The Langmuir isotherm model suggests single-layer surface sorption with no transmigration of the sorbate on the surface without interplaying the sorbed molecules and the uniform energy of adsorption [71]. Equation 4 describes the linear form of the Langmuir model and a plot of C_e/q_e against C_e . The slope and the interception are used to evaluate the maximum adsorption capacity (q_m) and the adsorption rate (K_L) , respectively.

$$\frac{c_e}{q_e} = \frac{1}{q_m \kappa_L} + \frac{c_e}{q_m} \tag{4}$$

Where K_L (L/mg) and q_m (mg/g) are Langmuir constants related to the rate of adsorption and adsorption capacity, respectively.

3.3.2 Freundlich isotherm

The isotherm of Freundlich is an empirical model based on the heterogeneous adsorption of surfaces and working environments with different energies [72]. Equation 5 illustrates the linear form of the isotherm Freundlich:

$$\log q_e = \log K_F + \frac{1}{n} \log C_e \tag{5}$$

where k_F ((mg/g) (L/mg)^{1/n}) and n are Freundlich constants relating respectively to the adsorption capacity of the adsorbate and the favorability of the adsorption process. If the value of 1/n is less than 1, the adsorption is favorable.

Table 3 includes a description of all phenol adsorption parameters and coefficients (R^2) for BFS-ACs. The adsorption strength or heterogeneity of the surface of the adsorption is measured with Freundlich. The slop 1/n is ranging from 0 to 1 and the surface is becoming more heterogenic when the value of 1/n extends the zero. A 1/n lower value indicates a normal Freundlich isotherm, whereas a 1/n higher than 1 shows more heavy sorption [73, 74].

The adsorption findings have shown 1/n for ZnCl₂, H₃PO₄, and KOH respectively at 0.205, 0,148, and 0.421, indicating favorable conditions of adsorption in this sample. It was observed that H₃PO₄ showed more affinity and heterogeneity than ZnCl₂ and KOH. Based on our findings, for each of the three produced activates the models of Langmuir were better suited for experimental data with higher R², showing that the adsorption process was on a uniform surface and that phenol was not transmigrated. The adsorbent was subsequently monolayered by the phenol adsorption in the adsorbent.

Table 3: Isotherm model parameters and correlation coefficients of phenol adsorption onto BFS-ACs

	Langmuir parameters			Freundlich parameters			
Adsorbent	$K_L(L/mg)$	$q_m (\text{mg/g})$	\mathbb{R}^2	$K_F (mg/g)(L/mg)^{1/n}$	1/n (L/mg)	n	\mathbb{R}^2
ZnCl ₂	0.0542	13.495	0.9515	4.026	0.205	4.863	0.7583
H_3PO_4	0.0385	9.505	0.9697	3.529	0.148	6.752	0.7233
KOH	0.0285	34.482	0.9336	2.773	0.421	2.375	0.8517

The Langmuir model also shows that the maximum adsorption rates (q_m) for ZnCl₂, H₃PO₄, and KOH were 13.49 mg/g, 9.505 mg/g, and 34.48 mg/g, respectively. These findings agree well with the experimental results, which also revealed that the adsorption process was in line with the Langmuir model.

3.4 Adsorption Kinetic Studies

The time-dependent experimental data were evaluated to investigate the rate-limiting step by adapting them to different Kinetics models, namely the pseudo-first-order model and the pseudo-second-order model. Linear forms of pseudo-first-order and pseudo-second-order kinetic equations are represented by Equations (6) and (7), respectively.

$$ln(q_e - q_t) = ln \, q_e - k_1 \, t \tag{6}$$

$$\frac{t}{q_t} = \frac{1}{(k_2 q_e^2)} + \frac{1}{q_e} t \tag{7}$$

where k_l (min⁻¹) and k_2 (g/min/mg) are the rates constant of the pseudo-first-order and pseudo-second-order adsorption, and q_t (mg/g) is the amounts of phenol adsorbed onto BFS-ACs at any time t (min).

The pseudo-first-order equations were compiled for different initial phenol concentrations. The slope and interception of the

plots $ln(q_e-q_t)$ against t have been used to determine the value of the first-order rate constant (k_1) and equilibrium adsorption capability (q_e) . Whereas the slopes and intercepts of the t/qt vs. t were used to determine the pseudo-second-order adsorption rate constant (k_2) and equilibrium adsorption capacity (q_e) . The derived kinetic parameters of the pseudo-first-order and pseudosecond-order are described in Table 4, which showed that no special trends were followed by the pseudo-first-order constant rate values and the adsorption capacities $(q_e \ cal)$ was very different and not by the experimental results, and the pseudo-firstorder model correlation coefficients (R²) were low values. On the other hand, for all initial concentrations of the various carbons, the correlation coefficients (R²) of the pseudo-second-order model are equal to or similar to 1, suggesting that the experimental kinetic results fitted better with the pseudo-secondorder model. Moreover, the calculated equilibrium adsorption capabilities ($q_e cal$) of the second-order equations are very similar to experimental $(q_e \ exp)$ equilibrium adsorption capacities, indicating that the second-order models are better suited to phenol kinetics and chemisorption may be the rate-limiting stage of the phenol in BFS-ACs. Due to the lower competition of sorption sites at lower concentrations, the rate of constant values (k^2) decreases with the initial phenol concentration increasing [75].

Table 4: Kinetic Model Parameters and Correlation Coefficients for Adsorption of phenol onto synthesized BFS-ACs

Adsorbent	C_{θ} (ppm)	$q_e \exp (\text{mg/g})$ -	Pseudo-first-order kinetics			Pseudo-second-order kinetics		
Ausorbent			qe cal (mg/g)	<i>k</i> ₁ (/min)	\mathbb{R}^2	qe cal (mg/g)	k ₂ (g/min/mg)	\mathbb{R}^2
	50	4.524	0.0081	0.0258	0.5302	4.526	1.1015	1
	100	8.392	0.0012	0.0257	0.3629	8.396	1.3906	1
$ZnCl_2$	200	12.741	0.9328	0.0474	0.819	12.820	0.0914	0.9999
	400	10.115	0.2061	0.0366	0.6168	10.152	0.1714	0.9998
	600	14.278	0.1927	0.032	0.6155	14.306	0.1954	0.9998
	50	4.751	0.0169	0.0217	0.5502	4.768	0.3922	1
	100	7.941	0.0019	0.0398	0.4437	7.949	0.9768	1
KOH	200	13.416	0.6622	0.0886	0.7662	13.458	0.1189	1
	400	25.952	0.3694	0.1052	0.6973	25.974	0.1398	0.9999
	600	36.91	6.0841	0.0926	0.8001	37.037	0.0389	0.9998
	50	4.281	0.0069	0.0281	0.7045	4.282	1.7038	1
	100	6.177	0.0017	0.0308	0.4524	6.184	1.0849	1
H_3PO_4	200	7.261	0.0389	0.0394	0.7296	7.272	0.5401	0.9999
	400	7.861	0.0566	0.0312	0.7937	7.867	0.5628	0.9998
	600	9.77	0.1295	0.0408	0.8261	9.794	0.3130	0.9996

To compare the effectiveness of BFS-AC to remove phenol in an aqueous solution, a comparison with other adsorbents was performed. Table 5 represents a comparison of the maximum adsorption capacity (q_m) of produced AC derived from baobab fruit shell, prepared in this work, with other adsorbents values reported in the literature. As observed, the maximum adsorption capacity differs in their values for activated carbons of different precursors. Moreover, it can be seen that BFS-AC appears to be a promising phenol removal adsorbent as it represents the third greatest adsorption capacity among the 16 adsorbents shown in Table 5.

Table 5: Comparison between BFS-ACs and other absorbents used for phenol adsorption

Adsorbent	Adsorption capacity (mg/g)	References
Activated red mud	1.580	[76]
AC derived from sewage sludge	30.1	[77]
AC derived from rice husk	27.5	[78]
Pyrolytic tire char	51.9	[79]
AC derived from fox nutshell	75.37	[42]
Bentonite	8.435	[80]
Kaolin	2.351	[80]
Zeolite	32.6	[81]
Porous clay	14.5	[82]
Calcined magnesium-zinc- Aluminium layered double hydroxide clay	12	[83]
Bagasse fly ash	23.832	[69]
Silica derived from rice Husk (SRH)	3.0	[84]
Bentonite	1.712	[85]
Amnerlite XAD-16 resin	1.5029	[78]
AC derived from peanut shell	21.0	[86]
AC derived from baobab fruit Shell	36.90	This Study

4 Conclusions

This study aimed to investigate activated carbon performance, prepared from BFS, using different activating agents with an impregnation ratio of 1:1 at an activation temperature of 500 °C for 1 h. It was found that the highest BET surface area of the obtained BFS-ACs samples can reach 1029.435 mg/g using KOH. Batch adsorption studies have been carried out using prepared BFS-ACs to remove phenol from aqueous solutions. It was revealed that the pseudo-second-order kinetic model better described the sorption data. The adsorption isotherm studies revealed that the Langmuir adsorption isotherm model adequately described the phenol onto KOH-AC, and it was found that 36.90 mg/g was the maximum adsorption capacity. More than 95.02 % phenol could be absorbed by KOH-AC within the initial 15 min. Removal of phenolic compounds by activated carbon derived from BFS was found favorable, and thus, BFS-ACs may be regarded as alternative commercial absorbents to remove phenolic compounds from the industrial wastewater.

Acknowledgment

The authors are grateful to the Department of Biotechnology Engineering, Faculty of Engineering, International Islamic University Malaysia for providing continuous support to the research at hand.

Ethical issue

Authors are aware of and comply with, best practices in publication ethics specifically about authorship (avoidance of guest authorship), dual submission, manipulation of figures, competing interests, and compliance with policies on research ethics. Authors adhere to publication requirements that submitted work is original and has not been published elsewhere in any language.

Competing interests

The authors declare that no conflict of interest would prejudice the impartiality of this scientific work.

Authors' contribution

All authors of this study have a complete contribution for data collection, data analyses, and manuscript writing.

References

- [1] Sokeng AJT, Sobolev AP, Di Lorenzo A, et al. Metabolite characterization of powdered fruits and leaves from Adansonia digitata L. (baobab): A multi-methodological approach. *Food Chem* 2019; 272: 93–108. https://doi.org/10.1016/j.foodchem.2018.08.030
- [2] Bazrafshan E, Amirian P, Mahvi AH, et al. Application of adsorption process for phenolic compounds removal from aqueous environments: A systematic review. *Glob Nest J* 2016; 18: 146–163. https://doi.org/10.30955/gnj.001709
- [3] Abd Gami A, Abd. Shukor M, Abdul Khalil K, et al. Phenol and phenolic compounds toxicity. J Environ Microbiol Toxicol 2014; 2: 11–23
- [4] Richard D, Delgado Núñez M de L, Schweich D. Adsorption of complex phenolic compounds on active charcoal: Adsorption capacity and isotherms. *Chem Eng J* 2009; 148: 1–7. https://doi.org/10.1016/j.cej.2008.07.023
- [5] Basha K, Rajendran A, Thangavelu V. Recent advances in the biodegradation of phenol: a review. Asian J Exp Biol Sci 2010; 1: 219–234.
- [6] Rashed MN. Adsorption Technique for the Removal of Organic Pollutants from Water and Wastewater. Org Pollut - Monit Risk Treat. Epub ahead of print 2013. https://doi.org/10.5772/54048
- [7] Yan KZ, Zaini MAA, Arsad A, et al. Rubber seed shell based activated carbon by physical activation for phenol removal. *Chem Eng Trans* 2019; 72: 151–156. https://doi.org/10.3303/CET1972026
- [8] Caetano M, Valderrama C, Farran A, et al. Phenol removal from aqueous solution by adsorption and ion exchange mechanisms onto polymeric resins. *J Colloid Interface Sci* 2009; 338: 402–409. https://doi.org/10.1016/j.jcis.2009.06.062
- [9] Ochando-Pulido JM, González-Hernández R, Martinez-Ferez A. On the effect of the operating parameters for two-phase olive-oil washing wastewater combined phenolic compounds recovery and reclamation by novel ion exchange resins. Sep Purif Technol 2018; 195: 50–59. https://doi.org/10.1016/j.seppur.2017.11.075
- [10] Víctor-Ortega MD, Ochando-Pulido JM, Martínez-Ferez A. Performance and modeling of continuous ion exchange processes for phenols recovery from olive mill wastewater. *Process Saf Environ Prot* 2016; 100: 242–251. https://doi.org/10.1016/j.psep.2016.01.017
- [11] Mohammadi S, Kargari A, Sanaeepur H, et al. Phenol removal from industrial wastewaters: a short review. *Desalin Water Treat* 2015: 53: 2215–2234.

- https://doi.org/10.1080/19443994.2014.883327
- [12] Peings V, Frayret J, Pigot T. Mechanism for the oxidation of phenol by sulfatoferrate(VI): Comparison with various oxidants. *J Environ Manage* 2015; 157: 287–296. https://doi.org/10.1016/j.jenvman.2015.04.004
- [13] Jiang J, Gao Y, Pang SY, et al. Understanding the role of manganese dioxide in the oxidation of phenolic compounds by aqueous permanganate. *Environ Sci Technol* 2015; 49: 520–528. https://doi.org/10.1021/es504796h
- [14] Ogando FIB, Aguiar CL de, Viotto JVN, et al. Removal of phenolic, turbidity and color in sugarcane juice by electrocoagulation as a sulfur-free process. *Food Res Int* 2019; 122: 643–652. https://doi.org/10.1016/j.foodres.2019.01.039
- [15] Jeong H, Lee J, Ju YM, et al. Using electro-coagulation treatment to remove phenolic compounds and furan derivatives in hydrolysates resulting from pilot-scale supercritical water hydrolysis of Mongolian oak. *Renew Energy* 2019; 138: 971–979. https://doi.org/10.1016/j.renene.2019.01.115
- [16] Liu J, Xie J, Ren Z, et al. Solvent extraction of phenol with cumene from wastewater. *Desalin Water Treat* 2013; 51: 3826–3831. https://doi.org/10.1080/19443994.2013.796993
- [17] Sharma NK, Philip L. Effect of cyanide on phenolics and aromatic hydrocarbons biodegradation under anaerobic and anoxic conditions. *Chem Eng J* 2014; 256: 255–267. https://doi.org/10.1016/j.cej.2014.06.070
- [18] Bedoui A, Saad MEK, Elaloui E, et al. Anodic oxidation of onitrophenol on BDD electrode: Variable effects and mechanisms of degradation. *J Hazard Mater* 2013; 250–251: 447–453. https://doi.org/10.1016/j.jhazmat.2013.02.027
- [19] Dalang S, Tuah PM. Removal of Phenol by Zeolite. *Trans Sci Technol* 2016; 3: 107–113.
- [20] Sharan R, Singh G, Gupta SK. Adsorption of Phenol from Aqueous Solution onto Fly Ash from a Thermal. 2009; 267–279.
- [21] Djebbar M, Djafri F, Bouchekara M, et al. Adsorption of phenol on natural clay. Appl Water Sci 2012; 2: 77–86. https://doi.org/10.1007/s13201-012-0031-8
- [22] Tadda MA, Ahsan A, Shitu A, et al. A Review On Activated Carbon: Process, Application And Prospects. J Adv Civ Eng Pract Res 2016; 2: 7–13. https://doi.org/10.1016/B978-1-59-749641-4.00015-1
- [23] Chaliha S, Bhattacharyya KG. Catalytic wet oxidation of 2-chlorophenol, 2,4-dichlorophenol and 2,4,6-trichlorophenol in water with Mn(II)-MCM41. Chem Eng J 2008; 139: 575–588. https://doi.org/10.1016/j.cej.2007.09.006
- [24] Poulopoulos SG, Nikolaki M, Karampetsos D, et al. Photochemical treatment of 2-chlorophenol aqueous solutions using ultraviolet radiation, hydrogen peroxide and photo-Fenton reaction. *J Hazard Mater* 2008; 153: 582–587. https://doi.org/10.1016/j.jhazmat.2007.09.002
- [25] Villegas LGC, Mashhadi N, Chen M, et al. A Short Review of Techniques for Phenol Removal from Wastewater. Curr Pollut Reports 2016; 2: 157–167. https://doi.org/10.1007/s40726-016-0035-3
- [26] Gao R, Wang J. Effects of pH and temperature on isotherm parameters of chlorophenols biosorption to anaerobic granular sludge. *J Hazard Mater* 2007; 145: 398–403. https://doi.org/10.1016/j.jhazmat.2006.11.036
- [27] Jawad AH, Sabar S, Ishak MAM, et al. Microwave-assisted preparation of mesoporous-activated carbon from coconut (Cocos nucifera) leaf by H3PO4 activation for methylene blue adsorption. Chem Eng Commun 2017; 204: 1143–1156. https://doi.org/10.1080/00986445.2017.1347565
- [28] González-García P. Activated carbon from lignocellulosics precursors: A review of the synthesis methods, characterization techniques and applications. *Renew Sustain Energy Rev* 2018; 82: 1393–1414. https://doi.org/10.1016/j.rser.2017.04.117
- [29] Mohammed J, Nasri NS, Ahmad Zaini MA, et al. Adsorption of benzene and toluene onto KOH activated coconut shell based

- carbon treated with NH3. *Int Biodeterior Biodegrad* 2015; 102: 245–255. https://doi.org/10.1016/j.ibiod.2015.02.012
- [30] Kosha S, Parmar A. Physico-chemical characteristics of Activated Carbon prepared from coconut shell. Int J Latest Eng Res Appl 2018; 3: 27–31.
- [31] Deng S, Hu B, Chen T, et al. Activated carbons prepared from peanut shell and sunflower seed shell for high CO2 adsorption. Adsorption 2015; 21: 125–133. <u>https://doi.org/10.1007/s10450-015-9655-y</u>
- [32] AL-Othman ZA, Ali R, Naushad M. Hexavalent chromium removal from aqueous medium by activated carbon prepared from peanut shell: Adsorption kinetics, equilibrium and thermodynamic studies. *Chem Eng J* 2012; 184: 238–247. https://doi.org/10.1016/j.cej.2012.01.048
- [33] Sha Y, Lou J, Bai S, et al. Facile preparation of nitrogen-doped porous carbon from waste tobacco by a simple pre-treatment process and their application in electrochemical capacitor and CO2 capture. Mater Res Bull 2015; 64: 327–332. https://doi.org/10.1016/j.materresbull.2015.01.015
- [34] Ghouma I, Jeguirim M, Dorge S, et al. Activated carbon prepared by physical activation of olive stones for the removal of NO2 at ambient temperature. *Comptes Rendus Chim* 2015; 18: 63– 74. https://doi.org/10.1016/j.crci.2014.05.006
- [35] Alabadi A, Razzaque S, Yang Y, et al. Highly porous activated carbon materials from carbonized biomass with high CO2 capturing capacity. *Chem Eng J* 2015; 281: 606–612. https://doi.org/10.1016/j.cej.2015.06.032
- [36] García JR, Sedran U, Zaini MAA, et al. Preparation, characterization, and dye removal study of activated carbon prepared from palm kernel shell. *Environ Sci Pollut Res* 2018; 25: 5076–5085. https://doi.org/10.1007/s11356-017-8975-8
- [37] Ameen ESM. Production of powdered activated carbon from oil palm empty fruit bunch for removal of phenol and treatment of palm oil mill final effluent. (Doctoral dissertation, Kulliyyah of Engineering, International Islamic University Malaysia), 2010.
- [38] Ahmad Zaini MA, Ali AH. Adsorptive characteristics and microwave dielectric properties of oil palm empty fruit bunch-based activated carbons for dye removal. *Malaysian J Fundam Appl Sci* 2018; 14: 241–245. https://doi.org/10.11113/mjfas.v14n2.1083
- [39] Nabais JMV, Laginhas CEC, Carrott PJM, et al. Production of activated carbons from almond shell. Fuel Process Technol 2011; 92: 234–240. https://doi.org/10.1016/j.fuproc.2010.03.024
- [40] Alau KK, Gimba CE, Kagbu JA. Preparation of Activated Carbon from Neem (Azadirachta indica) Husk by Chemical Activation with H3PO4, KOH and ZnCl 2. Arch Appl Sci Res 2010; 2: 451–455.
- [41] Prahas D, Kartika Y, Indraswati N, et al. Activated carbon from jackfruit peel waste by H3PO4 chemical activation: Pore structure and surface chemistry characterization. *Chem Eng J* 2008; 140: 32–42. https://doi.org/10.1016/j.cej.2007.08.032
- [42] Kumar A, Jena HM. Removal of methylene blue and phenol onto prepared activated carbon from Fox nutshell by chemical activation in batch and fixed-bed column. *J Clean Prod* 2016; 137: 1246–1259. https://doi.org/10.1016/j.jclepro.2016.07.177
- [43] Daffalla SB, Mukhtar H, Shaharun MS. Properties of activated carbon prepared from rice husk with chemical activation. *Int J Glob Environ Issues* 2012; 12: 107–129. https://doi.org/10.1504/IJGENVI.2012.049375
- [44] Vunain E, Kenneth D, Timothy B. Synthesis and characterization of low-cost activated carbon prepared from Malawian baobab fruit shells by H 3 PO 4 activation for removal of Cu (II) ions: equilibrium and kinetics studies. *Appl Water Sci* 2017; 7: 4301–4319. https://doi.org/10.1007/s13201-017-0573-x
- [45] Vunain E, Biswick T. Adsorptive removal of methylene blue from aqueous solution on activated carbon prepared from Malawian baobab fruit shell wastes: Equilibrium, kinetics and thermodynamic studies and thermodynamic studies. Sep Sci Technol 2018; 54: 27– 41. https://doi.org/10.1080/01496395.2018.1504794

- [46] Kabbashi NA, Mirghani MES, Alam MZ, et al. Characterization of the Baobab fruit shells as adsorption material. *Int Food Res J* 2017; 24: 472–474.
- [47] Nadavala SK, Che Man H, Woo H-S. Biosorption of Phenolic Compounds from Aqueous Solutions using Pine (Pinus densiflora Sieb) Bark Powder. *BioResources* 2014; 9: 5155–5174. https://doi.org/10.15376/biores.9.3.5155-5174
- [48] Ahmed MJ, Dhedan SK. Recommended articles Equilibrium isotherms and kinetics modeling of methylene blue adsorption on agricultural wastes- based activated carbons. Fluid Phase Equilib 2012: 9–14
- [49] Africa P. Baobab (Adansonia digitata L.) Fruit Pulp Powder Production Capacity and Sustainability in Southern Africa Prepared. Pretoria, South Africa Briza Publ 2008; 1–8.
- [50] Ismail BB, Pu Y, Fan L, et al. Science of the Total Environment Characterizing the phenolic constituents of baobab (Adansonia digitata) fruit shell by LC-MS / QTOF and their in vitro biological activities. Sci Total Environ 2019; 694: 133387. https://doi.org/10.1016/j.scitotenv.2019.07.193
- [51] Xu Z, Sun Z, Zhou Y, et al. Insights into the pyrolysis behavior and adsorption properties of activated carbon from waste cotton textiles by FeCl3-activation. *Colloids Surfaces A Physicochem Eng Asp* 2019; 582: 123934. https://doi.org/10.1016/j.colsurfa.2019.123934
- [52] Suárez-García F, Martínez-Alonso A, Tascón JMD. Pyrolysis of apple pulp: Chemical activation with phosphoric acid. *J Anal Appl Pyrolysis* 2002; 63: 283–301. https://doi.org/10.1016/S0165-2370(01)00160-7
- [53] Salas-Enríquez BG, Torres-Huerta AM, Conde-Barajas E, et al. Activated carbon production from the Guadua amplexifolia using a combination of physical and chemical activation. *J Therm Anal Calorim* 2016; 124: 1383–1398. https://doi.org/10.1007/s10973-016-5238-8
- [54] Al-Khatib MFR, Munjid M. Production of activated carbon from palm oil empty fruit bunch by chemical activation. In: Current research and developments in biotechnology engineering at IIUM. IIUM Press, Kuala Lumpur, 2011, pp. 209–216.
- [55] American Society for Testing and Materials. Standard for Method for Moisture in Activated Carbon ASTM D 2867-91. Philadelphia: PA: ASTM Committee on Standards, 1991.
- [56] Milne, T., Brennan, A. H., & Glenn BH. Sourcebook of Methods of Analysis for Biomass and Biomass Conversion Processes. (1990).
- [57] Mona S, Kaushik A, Kaushik CP. Biosorption of reactive dye by waste biomass of Nostoc linckia. *Ecol Eng* 2011; 37: 1589–1594. https://doi.org/10.1016/j.ecoleng.2011.04.005
- [58] Abdullah AH, Kassim A, Zainal Z, et al. Preparation and Characterization of Activated Carbon from Gelam Wood Bark (Melaleuca cajuputi). Malaysian J Anal Sci 2001; Vol. 7: 65–68.
- [59] Brunauer S, Emmett PH, Teller E. Surface area measurements of activated carbon, silica gels and other adsorbents. *J Am Chem Soc* 1938; 60: 309–319.
- [60] Xie B, Qin J, Wang S, et al. Adsorption of Phenol on Commercial Activated Carbons: Modelling and Interpretation. Int J Environ Res Public Health; 17. Epub ahead of print 2020. https://doi.org/10.3390/ijerph17030789
- [61] Marsh H, Rodríguez F. Activated Carbon. Elsevier, (2006).
- [62] Puziy AM, Poddubnaya OI, Martínez-Alonso A, et al. Surface chemistry of phosphorus-containing carbons of lignocellulosic origin. Carbon N Y 2005; 43: 2857–2868. https://doi.org/10.1016/j.carbon.2005.06.014
- [63] Vunain E, Kenneth D, Biswick T. Synthesis and characterization of low-cost activated carbon prepared from Malawian baobab fruit shells by H3PO4 activation for removal of Cu(II) ions: equilibrium and kinetics studies. *Appl Water Sci* 2017; 7: 4301–4319. https://doi.org/10.1007/s13201-017-0573-x
- [64] Bohli T, Ouederni A, Fiol N, et al. Evaluation of an activated carbon from olive stones used as an adsorbent for heavy metal

- removal from aqueous phases. *Comptes Rendus Chim* 2015; 18: 88–99. https://doi.org/10.1016/j.crci.2014.05.009
- [65] Köse TE, Demiral H, Öztürk N. Adsorption of boron from aqueous solutions using activated carbon prepared from olive bagasse. *Desalin Water Treat* 2011; 29: 110–118. https://doi.org/10.5004/dwt.2011.2091
- [66] Salame II, Bandosz TJ. Role of surface chemistry in adsorption of phenol on activated carbons. J Colloid Interface Sci 2003; 264: 307–312. https://doi.org/10.1016/S0021-9797(03)00420-X
- [67] Zhang D, Huo P, Liu W. Behavior of phenol adsorption on thermal modified activated carbon. *Chinese J Chem Eng* 2016; 24: 446–452. https://doi.org/10.1016/j.cjche.2015.11.022
- [68] Hameed BH, Rahman AA. Removal of phenol from aqueous solutions by adsorption onto activated carbon prepared from biomass material. J Hazard Mater 2008; 160: 576–581. https://doi.org/10.1016/j.jhazmat.2008.03.028
- [69] Srivastava VC, Swamy MM, Mall ID, et al. Adsorptive removal of phenol by bagasse fly ash and activated carbon: Equilibrium, kinetics and thermodynamics. *Colloids Surfaces A Physicochem Eng Asp* 2006; 272: 89–104. https://doi.org/10.1016/j.colsurfa.2005.07.016
- [70] Gao J, Kong D, Wang Y, et al. Production of mesoporous activated carbon from tea fruit peel residues and its evaluation of methylene blue removal from aqueous solutions. *BioResources* 2013; 8: 2145–2160. https://doi.org/10.15376/biores.8.2.2145-2160
- [71] Vimala R, Das N. Biosorption of cadmium (II) and lead (II) from aqueous solutions using mushrooms: A comparative study. *J Hazard Mater* 2009; 168: 376–382. https://doi.org/10.1016/j.jhazmat.2009.02.062
- [72] Kilic M, Apaydin-Varol E, Pütün AE. Adsorptive removal of phenol from aqueous solutions on activated carbon prepared from tobacco residues: Equilibrium, kinetics and thermodynamics. J Hazard Mater 2011; 189: 397–403. https://doi.org/10.1016/j.jhazmat.2011.02.051
- [73] Angin D, Altintig E, Köse TE. Influence of process parameters on the surface and chemical properties of activated carbon obtained from biochar by chemical activation. *Bioresour Technol* 2013; 148: 542–549. https://doi.org/10.1016/j.biortech.2013.08.164
- [74] Angin D. Utilization of activated carbon produced from fruit juice industry solid waste for the adsorption of Yellow 18 from aqueous solutions. *Bioresour Technol* 2014; 168: 259–266. https://doi.org/10.1016/j.biortech.2014.02.100
- [75] Kumar PS, Ramalingam S, Sathishkumar K. Removal of methylene blue dye from aqueous solution by activated carbon prepared from cashew nut shell as a new low-cost adsorbent. *Korean J Chem Eng* 2011; 28: 149–155. https://doi.org/10.1007/s11814-010-0342-0
- [76] Shirzad-Siboni M, Jafari SJ, Farrokhi M, et al. Removal of phenol from aqueous solutions by activated red mud: Equilibrium and kinetics studies. *Environ Eng Res* 2013; 18: 247–252. https://doi.org/10.4491/eer.2013.18.4.247
- [77] Sierra I, Iriarte-Velasco U, Cepeda EA, et al. Preparation of carbon-based adsorbents from the pyrolysis of sewage sludge with CO2. Investigation of the acid washing procedure. *Desalin Water Treat* 2016; 57: 16053–16065. https://doi.org/10.1080/19443994.2015.1075428
- [78] Shen Y, Fu Y. KOH-activated rice husk char via CO2 pyrolysis for phenol adsorption. *Mater Today Energy* 2018; 9: 397–405. https://doi.org/10.1016/j.mtener.2018.07.005
- [79] Makrigianni V, Giannakas A, Deligiannakis Y, et al. Adsorption of phenol and methylene blue from aqueous solutions by pyrolytic tire char: Equilibrium and kinetic studies. *J Environ Chem Eng* 2015; 3: 574–582. https://doi.org/10.1016/j.jece.2015.01.006
- [80] Alkaram UF, Mukhlis AA, Al-Dujaili AH. The removal of phenol from aqueous solutions by adsorption using surfactantmodified bentonite and kaolinite. *J Hazard Mater* 2009; 169: 324– 332. https://doi.org/10.1016/j.jhazmat.2009.03.153

- [81] Ghiaci M, Abbaspur A, Kia R, et al. Equilibrium isotherm studies for the sorption of benzene, toluene, and phenol onto organozeolites and as-synthesized MCM-41. Sep Purif Technol 2004; 40: 217–229. https://doi.org/10.1016/j.seppur.2004.03.001
- [82] Arellano-cárdenas S, Gallardo-velázquez T, Osorio-revilla G, et al. Adsorption of Phenol and Dichlorophenols from Aqueous Solutions by Porous Clay Heterostructure (PCH). Rev la Soc Química México 2005; 49: 287–291.
- [83] Tabana L, Tichapondwa S, Labuschagne F, et al. Adsorption of phenol fromwastewater using calcined magnesium-zinc-aluminium layered double hydroxide clay. *Sustain*; 12. Epub ahead of print 2020. DOI: 10.3390/su12104273. https://doi.org/10.3390/su12104273
- [84] Asgharnia H, Nasehinia H, Rostami R, et al. Phenol removal from aqueous solution using silica and activated carbon derived from rice husk. Water Pract Technol 2019; 14: 897–907. https://doi.org/10.2166/wpt.2019.072
- [85] Banat FA, Al-Bashir B, Al-Asheh S, et al. Adsorption of phenol by bentonite F.A. *Diagn Imaging* 1999; 107: 391–398.
- [86] Villar da Gama BM, Elisandra do Nascimento G, Silva Sales DC, et al. Mono and binary component adsorption of phenol and cadmium using adsorbent derived from peanut shells. *J Clean Prod* 2018; 201: 219–228. https://doi.org/10.1016/j.jclepro.2018.07.291